Biosensors and Bioelectronics 144 (2019) 111534

Contents lists available at ScienceDirect

Biosensors and Bioelectronics

journal homepage: www.elsevier.com/locate/bios

Chemical nature of electrochemical activation of carbon electrodes

Yiwei Li[a,c], Juan Zhou[a], Jin Song[b,d], Xiaosheng Liang[b,e], Zhiping Zhang[a], Dong Men[a,**], Dianbing Wang[b], Xian-En Zhang[b,c,*]

[a] State Key Laboratory of Virology, Wuhan Institute of Virology, Chinese Academy of Sciences, Xiao Hong Shan No.44, Wuhan, 430071, China
[b] National Key Laboratory of Biomacromolecules, CAS Center for Biological Macromolecules, Institute of Biophysics, Chinese Academy of Sciences, 15 Datun Road, Chaoyang District, Beijing, 100101, China
[c] Graduate University of Chinese Academy of Sciences, No.19A Yuquan Road,Shijingshan District, Beijing, 100049, China
[d] State Key Laboratory of Chemical Resource Engineering, Beijing University of Chemical Technology, North Third Ring Road 15, Chaoyang District, Beijing, China
[e] Provincial Key Laboratory for Protection and Application of Special Plants in Wuling Area of China, College of Life Science, South-Central University for Nationalities, No. 182, Minyuan Road, Hongshan District, Wuhan, 430074, Hubei, China

ARTICLE INFO

Keywords:
Electrochemical activation
Carbonaceous electrode
Graphene
Electrochemical sensing

ABSTRACT

Electrochemical activation of carbonaceous electrodes is a common step in the preparation of high-performance electrochemical (bio-)sensors. The underlying mechanism has long been discussed but is, however, not yet fully understood. Here, we propose that electrochemical activation can produce graphene derivatives that largely enhance the electrochemical performance of carbonaceous electrodes using a carbon paste electrode or a carbon rod electrode as samples. Based on morphological, chemical and electrochemical evidence, we conclude that in the electrochemical activation of carbonaceous electrodes, graphene oxide or reduced graphene oxide could be generated *in situ*, which is the main reason for the enhancement of the electrode performance. Moreover, chemical and biological sensors made from electrochemically activated carbonaceous electrodes resemble their counterparts made from chemically prepared graphene-derivative-modified carbonaceous electrodes and even exhibit better performance. These findings could enable us to establish an efficient and predictable solution for graphene-related electrochemistry and surface chemistry.

1. Introduction

Electrochemical (bio)sensors show advantages in terms of selectivity, sensitivity, reliability, cost-effectiveness, ease of fabrication and so forth, for which carbonaceous electrode (CE) is a common and paramount transducer (Hosseini et al., 2014; Zeinali et al., 2017; Bojdi et al., 2014; Rahmani et al., 2018; Bagheri et al., 2015; Bojdi et al., 2015). To improve electrochemical sensing capability, a number of CE activation techniques were designed decades ago, such as mechanical polishing (Miller et al., 1981; Zak and Kuwana, 1982), chemical treatment (Taylor and Humffray, 1973), O_2 plasma (Evans et al., 1977) or laser treatment (Poon and McCreery, 1986), heating termination (Stutts et al., 1983; Dan et al., 1985), and electrochemical pretreatment (Blaedel and Jenkins, 1974; Engstrom and Strasser, 1984). Among these, electrochemical pretreatment is frequently used because it is more cost-effective and easier under mild processing conditions. In its early stages, researchers found that electrochemically activated CEs have better sensitivity (Hadi et al., 2006), reversibility (Falat and Cheng, 1982), reproducibility, stability (Wang and Peng, 1986) and reduced overpotential (Engstrom, 1982) compared with their precursors. After years of exploration, electrochemical pretreatment has evolved from an electrode-modification method to an electrode-fabrication technique (McCreery, 2008) and has been successfully used in electrodes made of various forms of carbon precursors (Santhiago et al., 2017; Wang et al., 1996; Xiang et al., 2014). The electrochemical activation mechanism of CEs has always attracted the attention of the electrochemical community. From a large amount of experimental evidence, the mechanism of electrode activation can be summarized as follows: i) introduction of electrochemically active oxygen-rich groups such as hydroxyls, carbonyls, carboxyls, epoxyls, and quinoidals on the electrode surface (Engstrom, 1982; Kepley and Bard, 1988; Cabaniss et al., 1985; Gunasingham and Fleet, 1982), ii) nanostructure produced on the electrode surface caused by an electrochemical etching effect (Cabaniss et al., 1985) or iii) production of defects/edge plane sites (Wang et al., 1996). Nevertheless, it is still daunting to quantitatively control the CEs with precisely predictable performance through existing

* Corresponding author. 15 Datun Road, Chaoyang District, Beijing, 100101, China.
** Corresponding author. Xiao Hong Shan No.44, Wuhan, China.
E-mail addresses: d.men@wh.iov.cn (D. Men), zhangxe@ibp.ac.cn (X.-E. Zhang).

https://doi.org/10.1016/j.bios.2019.111534
Received 19 June 2019; Received in revised form 20 July 2019; Accepted 23 July 2019
Available online 26 July 2019
0956-5663/

interpretations, primarily because the exact chemical nature of the CE electro-activation is not yet well understood (Santhiago et al., 2015).

In recent decades, carbon nano-materials such as C_{60}, carbon nanotubes (CNTs), and graphenes have been introduced to produce high-performance electrochemical sensors (Bai et al., 2017; Chen et al., 2016; Lee et al., 2016). Graphene materials can be produced directly from graphites by electrochemical treatment. Anodic activation of CEs results in the formation of a porous graphite oxide layer (Kepley and Bard, 1988), and electro-oxidized glassy carbon electrodes (GCEs) exhibit an electrochemical response similar to graphene oxide (GO) (Santhiago et al., 2015). Moreover, researchers have been trying to use electricity as a driving force for obtaining scalable GO sheets from graphite, although most processes require the help of oxidative acids, alkalis, surfactants, ionic liquids, high voltages, etc. (Pei et al., 2018; Matsumoto et al., 2015; Li et al., 2008) Inspired by this evidence, we speculate that the electrochemical activation of CEs may produce GO and reduced graphene oxide (rGO) on the electrode surface and that this may be an inherent property of electro-activation.

In the current study, we treated CEs with the typical electrochemical activation method. The change in the electrode surface was characterized both *in situ* and *ex situ*. We found the *in situ* formation of GO and rGO along with carbonaceous fragments (CFs) after electrochemical activation. The scheme and major findings are illustrated in Fig. 1. These findings may fully explain why electrochemical treatment can dramatically improve the performance of CEs and would stimulate the development of novel fabrication techniques for electrochemical (bio-) sensors and even batteries.

2. Materials and methods

All materials, reagents, experimental methods and instrumentations used throughout this study are described in detail in the Supporting information.

3. Results and discussion

3.1. Electrochemical treatment results for the production of GO and rGO-like structures on the surface of the carbon paste electrode

We chose a graphite-based carbon paste electrode (CPE) and carbon rod electrode (CRE) to verify our hypothesis. As shown in Supplementary Fig. 1, after electrochemical oxidation by cyclic voltammetry (CV) scanning (0–2.5 V), the CPE had a lustre similar to that of an oil slick on its surface. By further reducing the CV (− 1.5 to 0 V), it was found that the lustre disappeared. In the comparison groups, the lustre also appeared on the CPE modified by the chemically prepared GO (cGO) but not on the CPE modified by chemically prepared reduced graphene oxide (crGO).

The anodically and cathodically treated CPEs were first characterized *in situ* using scanning electron microscopy (SEM). Prior to electrochemical treatment, the pristine graphite particles were readily observed to be heterogeneously distributed (Fig. 2a). After electrochemical oxidation, most of the graphite particles disappeared, and the electrode surface structure was more uniform (Fig. 2b). However, in the enlarged views, the anodized CPE surface showed a rough topography. This phenomenon was in good agreement with previous reports using GCEs, graphitic carbon fibre, and graphite-based SPEs

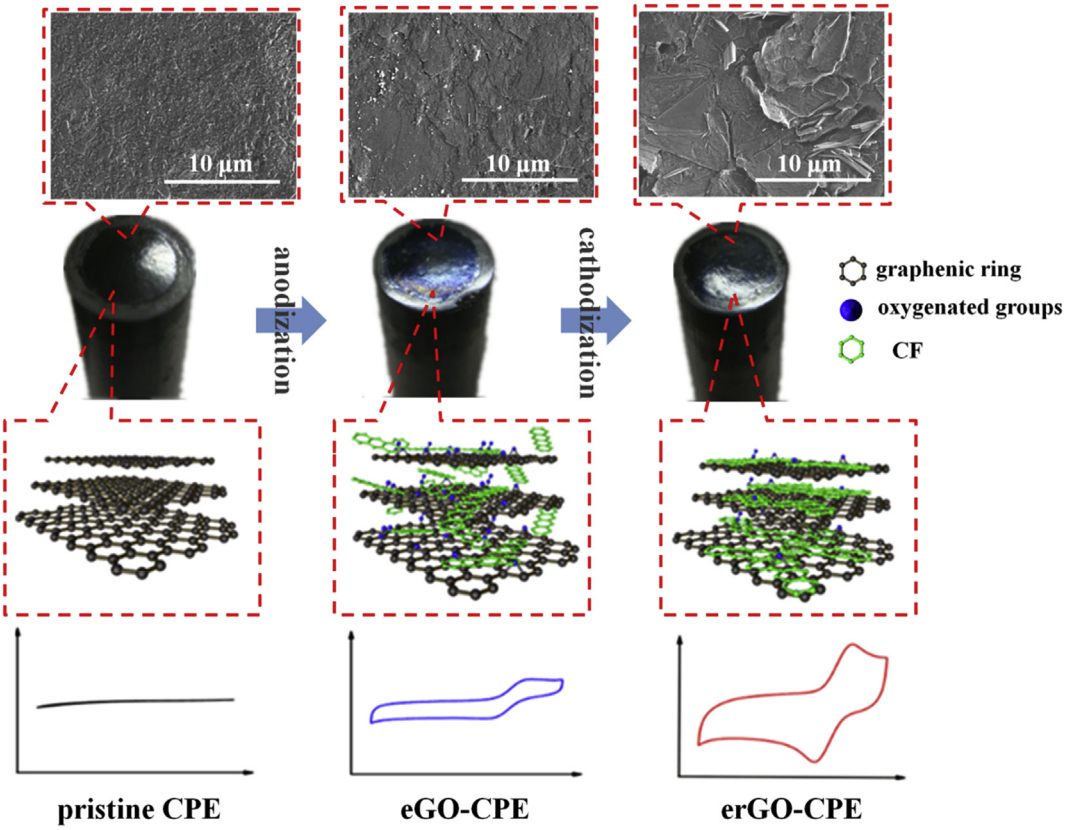

Fig. 1. Schematic diagram of chemical changes during the electrochemical activation of CEs. The pristine CE typically exhibited very limited electrochemical performances (such as sensitivity, stability, effective specific surface area, and reversibility). After proper anodization, the performances were significantly improved due to the *in situ* generation of graphene oxide sheets and some electrochemically active CFs on the electrode surface. When the electrode was further cathodized, its properties could be further altered or improved because of the *in situ* formation of the rGO layer, during which CFs were re-stacked and affected the performance. In the processes, microstructure changes can also captured as an evidence of surface material conversion.

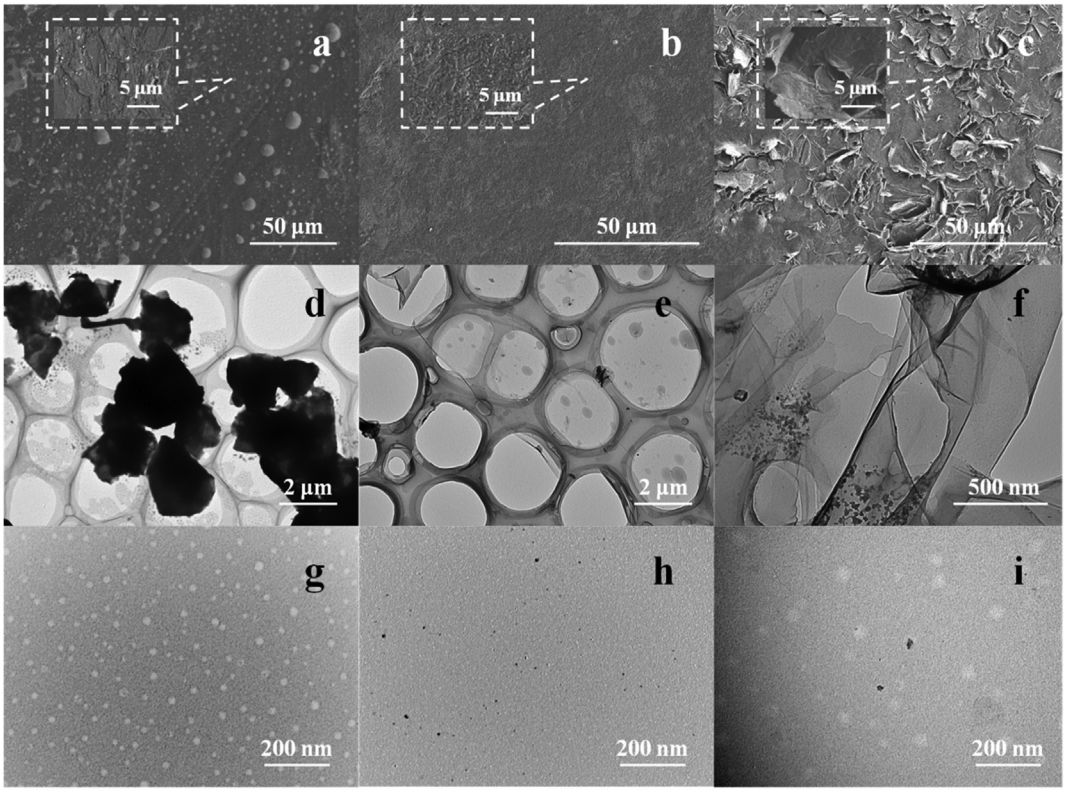

Fig. 2. SEM and TEM images of the pristine CPE, anodized CPE, and anodized-cathodized CPE. **a-c**, SEM images of pristine CPE composed of graphite particles and paraffin binder (a), CPE treated by electrochemical oxidation (b), and CPE further treated by electrochemical reduction (c). The insets show the magnified SEM views. **d-e**, TEM images of the transient ultrasonic stripping products from the samples in a-c, respectively. **g-i**, TEM images of the electrolyte solutions from the samples in a-c, respectively.

(Heiduschka et al., 1994; Cheng et al., 2011; Shuhao et al., 2013), which can be regarded as an indication of the dissociation of graphite particles (Lotya et al., 2009). The dramatic changes in surface roughness and the homogeneity of the electrodes were considered to be caused by the electrochemical etching effect under extreme potentials (Cheng et al., 2011).

After electrochemical oxidation, the reverse treatment, that is, electrochemical reduction, was performed by CV scanning (−1.5 to 0 V). A large number of fluffy layered structures were found on the electrode surface (Fig. 2c), indicating that the surface of the permanently anodized CPE was forced to rearrange by electrochemical reduction. A similar layered structure was reported for the crGO sample (Liu et al., 2011). We then characterized the structures by using transmission electron microscopy (TEM), atomic force microscopy (AFM), high-resolution transmission electron microscopy (HRTEM), Raman spectroscopy, Fourier transform infrared spectroscopy (FTIR), X-ray photoelectron spectroscopy (XPS), and UV–vis spectroscopy, which are usually necessary for the characterization of graphene derivatives.

In the TEM characterization, the pristine CPEs were treated by brief and weak ultrasonication and electrochemical treatment (Fig. 2d). As a result, the ultrasonic processing promoted the detachment of graphite particles from the electrode surface but had little effect on their dissociation. In contrast, the electrochemical treatment produced a monolayer or oligo-layer of material on the CPE surface (Fig. 2 e and f), suggesting that the electrochemical treatment causes the *in situ* dissociation of the bulky graphite particle into layered, graphene-like derivatives.

Based on the aforementioned facts, we assumed that the electrochemically produced graphene oxide (eGO) was synthesized *in situ* on the CE surface after anodizing and that the eGO was converted to electrochemically reduced graphene oxide (erGO) in a subsequent cathodic treatment.

Unexpectedly, when we traced the changes in the electrolyte solution by TEM, some small laminar structures were also found, which were not present before anodization and cathodization treatments (Fig. 2 g-i). They exhibited a distinct difference in the lateral size (on the order of tens of nanometres) compared with the ultrasonically stripped products of electrochemically treated CPE (on the order of microns). This feature made them very similar to the reported CFs with a graphenic structure and electrocatalytic activity (Rourke et al., 2011; Gusmão et al., 2016).

3.2. Characterization of the electrochemically treated CPE surface indicates the production of GO or rGO

We next verified the chemical nature of the electrochemically treated CPE surfaces, their stripped products, and CF-like structures. The Raman spectrum of the pristine CPE (Fig. 3) revealed a prominent G peak (1580 cm^{-1}) and a weak D peak (1323 cm^{-1}), which were mainly due to the in-plane vibrations of sp^2-bonded carbons and intrinsic structural defects[36], respectively. After electrochemical treatment, the I_D/I_G ratio, a well-recognized index associated with defect content (Ambrosi et al., 2014), increased significantly, indicating that both the anodized CPE and cathodically treated CPE after anodization (which we denoted as eGO-CPE and erGO-CPE) contain more edge plane sites/defects on their surfaces. These data were fully consistent with the SEM characterization results and a previous report (Thiruppathi et al., 2016). As shown in Fig. 3, the CPE anodized through 10 CV cycles showed a higher I_D/I_G ratio than that of the CPE that only experienced 5 CV cycles, implying that the surface properties of CEs can be controlled by the degree of electrochemical treatment. In addition, a 2D band (~2700 cm^{-1}) was found in all three types of samples and showed a significant red-shift compared to that found in

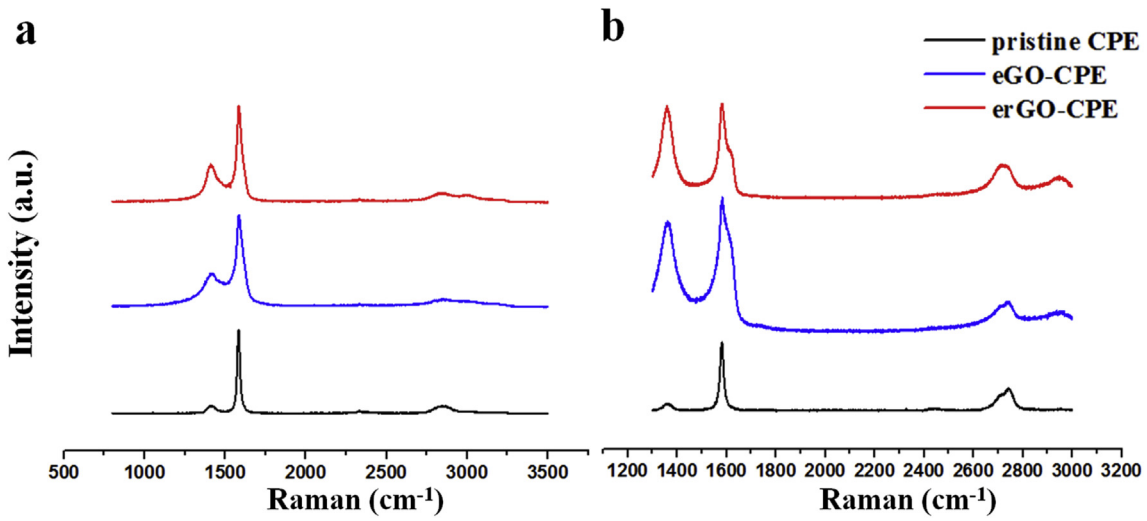

Fig. 3. *In situ* Raman spectral characteristics of pristine CPE, eGO-CPE, and erGO-CPE. **a**, CPEs before and after 5 cycles of oxidative CV scanning (0–2.5 V). **b**, CPEs before and after 10 cycles of oxidative CV scanning (0–2.5 V).

the > 10-layer graphite (~2720 cm^{-1}) (Buzaglo et al., 2016), suggesting that our samples obtained by the electrochemical treatment consisted mainly of mono- or few-layered graphene structures. The peak was attenuated after anodization, indicating the formation of defects during eGO production. However, the peak intensity increased and showed better symmetry after cathodization, implying recovery of the sp^2-bonded structures and removal of the defect sites (Thiruppathi et al., 2016; Yu et al., 2016). It was also found that a D + G band (~2910 cm^{-1}) was observed only after electrochemical treatment. The peak can be interpreted as the formation of CF or "nanographene", which is an important functional byproduct typically found in chemically generated graphenes (Gusmão et al., 2016; Thiruppathi et al., 2016).

To obtain a sufficient amount of nanostructures of small lateral dimensions present in the electrolyte, we separated them using a protocol associated with anodized CREs (Rourke et al., 2011). The TEM characterization results of this product (Supplementary Fig. 2) were in good agreement with the nanostructures found in the electrolyte solution, indicating an analogy between the two materials. We used this sample for the following characterization to investigate whether CFs function on the electrochemically treated CE surface. Moreover, the Raman spectral characterization of the purified CFs suggests their graphite properties (Supplementary Fig. 3).

We then used XPS analysis to obtain detailed information on the elemental and structural composition of the structures acquired from the electrochemical treatment. Based on the XPS survey scan results (Fig. 4a), significant changes between the pristine CPE, eGO-CPE, and erGO-CPE were concentrated in the C1s and O1s bands. The O1s spectra (Fig. 4b) showed an increase in oxygen abundance in eGO-CPE and a decrease in erGO-CPE. The deconvoluted XPS C1s spectra of the pristine CPE (Fig. 4c) showed a strong C=C peak (284.6 eV) and a C–C peak (285.2 eV) (Buzaglo et al., 2016; Yang et al., 2015; Parvez et al., 2016). After electrochemical oxidation, the intensity of the C=C peak decreased as the C–C peak increased, indicating an increase in sp^3 carbon and a decrease in sp^2 carbon. In addition, significant increases in carbon-bonded oxygen groups were observed, including the C–OH/C–O–C peak (286.5 eV) (Buzaglo et al., 2016; Yu et al., 2016) and C=O peak for carbonyl groups (287.9 eV), which indicates the introduction of oxygen-containing groups and the formation of eGO (Fig. 4d) (Parvez et al., 2016). After electrochemical reduction, sp^3 carbons were reduced, and sp^2 carbons were increased, implying the removal of defects/edge plane sites. These oxygen-carbon peaks declined sharply, indicating the removal of the oxygen-containing groups, as concluded from the O1s spectra (Fig. 4e). Interestingly, no significant change in carboxyl groups was detected throughout the electrochemical treatment, in contrast to widely reported synthesis of GO. This may be due to a low degree of electrochemical oxidation and, on the other hand, the absence of any strong acid and/or oxidant. The FTIR spectra (Supplementary Fig. 4 and Supplementary Note 1) also showed similar changes in the functional groups of CEs before and after electrochemical treatment. In addition, UV–vis spectroscopy of the ultrasonic products from eGO-CPEs showed similar UV–vis spectral behaviour compared with that of the cGO suspensions shown in Supplementary Fig. 5 and Supplementary Note 2.

We then used AFM and HRTEM to obtain more data confirming the chemical properties of the briefly ultrasonically exfoliated nanostructures. The AFM measurements of the ultrasonic stripping products from eGO-CPE and erGO-CPE (Fig. 4f and g) showed lateral dimensions similar to the TEM results described above. Moreover, the corresponding height measurements demonstrated that most ultrasonic exfoliated products were only approximately 1 nm thick, similar to a single layer of graphene derivative (Parvez et al., 2016). HRTEM images of the short ultrasonic stripping products from eGO-CPE and erGO-CPE (Fig. 4h–i) clearly presented ordered graphitic lattices. The SAED pattern obtained from the corresponding sample exhibited six typical reflection spots (inserts in Fig. 4j–k), demonstrating the well-ordered high crystallinity of single- and few-layer graphene sheets. We also identified the CF and found that the nanosized structure showed a lateral dimension and shape similar to what we observed in the electrolyte described above (Fig. 4l). A similar SAED dot matrix shown in Fig. 4j and k implies its graphenic trait. In addition, nothing was found in the HRTEM view of the sample from the identically treated CRE without electrochemical treatment. These data indicate that CFs are produced during the electrochemical oxidation of CEs. Fig. 4m shows the optimal structure of the CFs in this study. Theses CFs could be produced from two main routes. One is from the dissociation of graphite lattice, due to the inherent heterogeneity of the graphite lattice, some of the infinitesimal graphenic fragments would be exposed to the external environment in company with the dissociation process. The other is from the "cutting effect" of electricity, by which graphene layers could be lacerated into smaller flakes especially under oxidative electro-processing.

The data presented here clearly support the production of graphene derivatives from the electrochemically treated CE surface, which could be a very simple CE functionalization method.

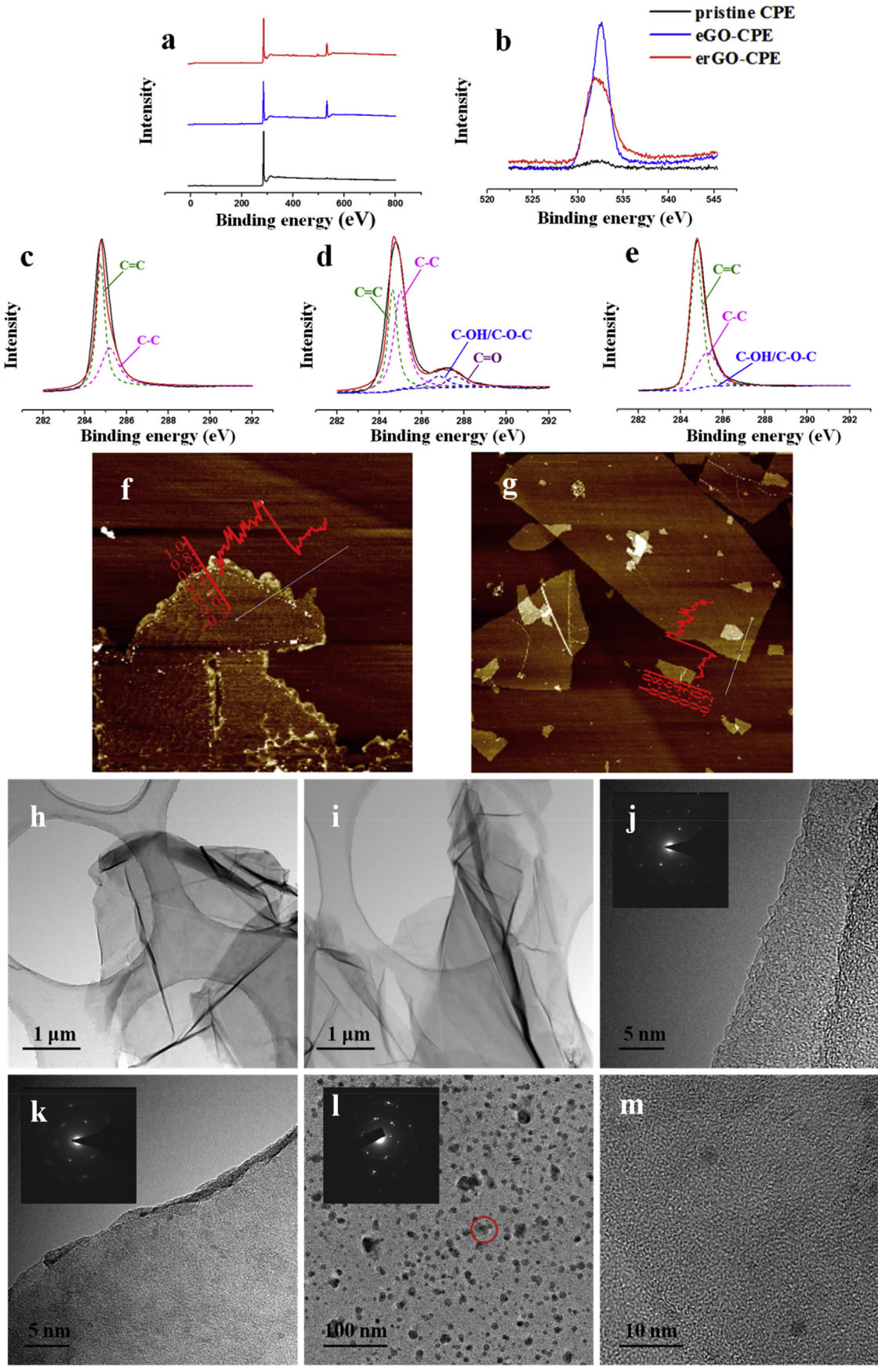

(caption on next page)

Fig. 4. XPS (a–e) and atomic-resolution microscopy (f–m) characterization of eGO-CPE, erGO-CPE, and CFs. **a**, XPS survey scan. **b**, XPS O1s spectra. **c-e**, XPS high-resolution C1s spectra of pristine CPE (c), eGO-CPE (d), and erGO-CPE (e). **f-g**, AFM images and height measurements of the ultrasonic stripping products from eGO-CPE (f) and erGO-CPE (g). **h-k**, HRTEM images (h, i) and corresponding selected area diffraction (SAED) patterns (j, k) of the ultrasonic stripping products from eGO-CPE (h, j) and erGO-CPE (i, k). **l-m**, HRTEM images of the base-washed product from eGO-CRE: **l)** a full view with an SAED pattern and **m)** a high-resolution view showing the crystallinity of the particles.

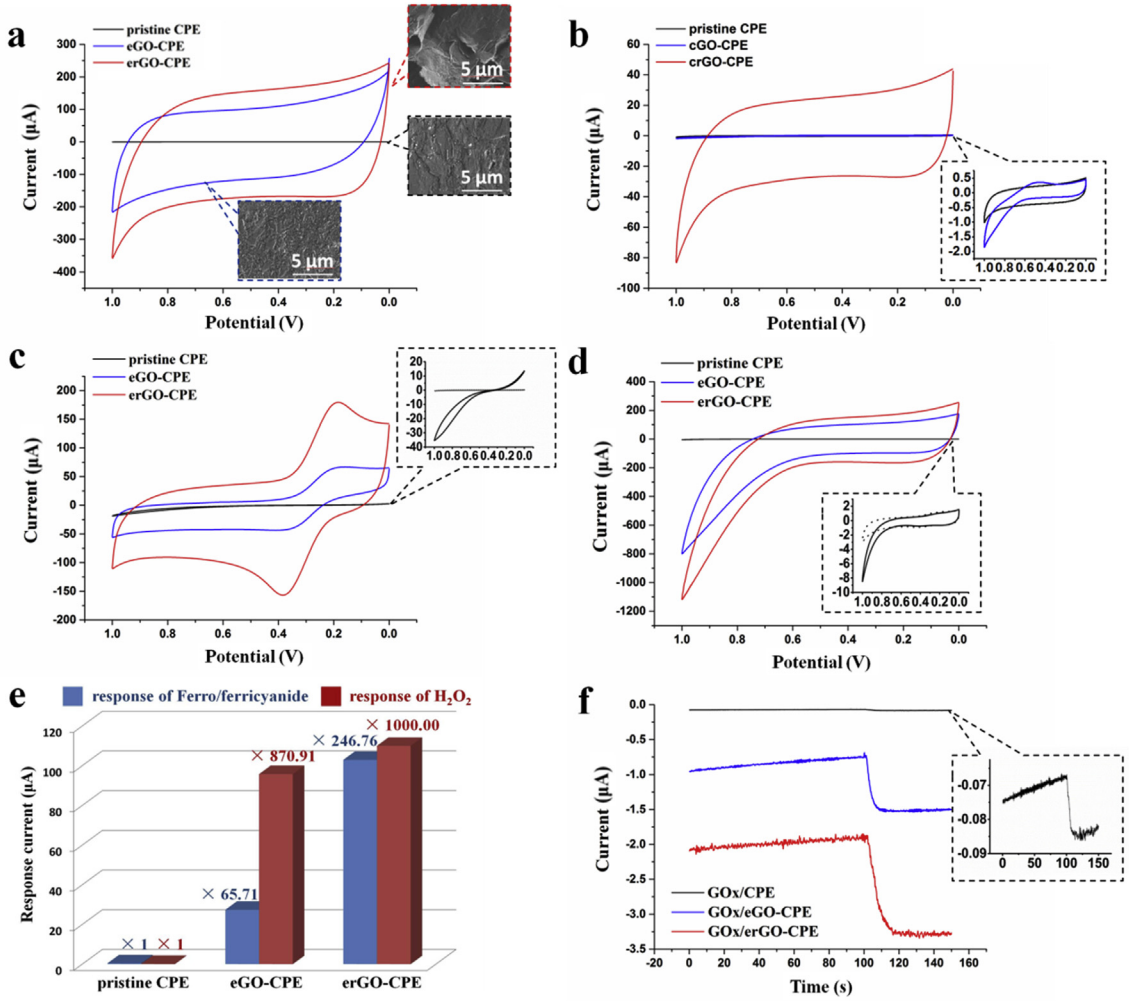

Fig. 5. Electrochemical characterization of the CPEs before and after electrochemical activation. **a**, CV responses in 0.1 M PBS (pH 7.0). The insets present photographs of the corresponding surface morphology captured by SEM (also please refer to Fig. 2a–c). **b**, CV responses of the CPEs modified by 0.1 mg/mL cGO suspension in 0.1 M PBS (pH 7.0). **c**, CV responses of the CPEs in 0.025 mM $[Fe(CN)_6]^{-3}$-$[Fe(CN)_6]^{-4}$ solution. **d**, CV responses of the CPEs in 1.0 mM H_2O_2 with 0.1 M PBS (pH 7.0). **e**, Bar graphs of sensitivity comparison based on the results from **d** and **e**. **f**, Amperometric responses of the GOx modified CPEs in 0.1 M PBS (pH 7.0) with and without 1.0 mM glucose.

3.3. Electrochemically treated CEs exhibit comparable electrochemical performance to graphene-modified CEs

It is necessary to investigate the electrochemical behaviours of electro-activated CPEs in both electrochemically inert and active electrolyte environments to thus compare them with their counterparts modified by chemically prepared graphene derivatives. As shown in Fig. 5a, the response current of the CPEs was very weak before anodization but dramatically increased after anodization. Two possibilities might account for this observation. First, production of GO/rGO and CFs during the electrochemical treatment led to an increase in the capacitance of the CE surface, as observed in previous studies (Lotya et al., 2009; Thiruppathi et al., 2016). The much higher amplified charging current obtained in our study also supports the notion that the graphene derivatives produced *in situ* are ideal super-capacitive materials (Shao et al., 2015). The significant capacitive effect may also result from the highly oxygenated CF particles described above, which were previously reported while studying the electrochemical properties of CFs collected from cGO sheets (Yang et al., 2013). Second, the dissociation of graphite particles (the etching effect) on the electrode surface led to an increase in the electrochemically active surface area (EASA) of the CE, as evidenced by our SEM results. We found that the difference in the response currents between cGO-CPE and pristine CPE was very limited (Fig. 5b) because graphene oxide itself was a comparatively insulating material (Liu et al., 2010). In contrast, eGO-CPE exhibited a greatly improved conductivity, which should not be caused by the *in situ* production of eGO, but for the etching effect of the anodization that had led to an increase in EASA.

As shown in Supplementary Fig. 6 and Supplementary Note 3, the electron transfer resistance (R_{ct}) elements of the pristine CPE and its counterparts were analysed. The results undoubtedly indicate the production of eGO and erGO upon eGO-CPE and erGO-CPE and the presence of the electro-etching effect upon eGO-CPE. For CPE, eGO-CPE, and erGO-CPE, the EASA values of the electrodes were estimated to be

0.073 ± 0.0006 cm^2, 0.125 ± 0.0010 cm^2, and 0.131 ± 0.0010 cm^2, respectively (Supplementary Fig. 7 and Supplementary Note 4). Compared to the pristine CPE, eGO-CPE and erGO-CPE increased by ~71% and ~79%, respectively, indicating that the electrochemical activation processes contribute to the EASA of the electrode and that anodization is the predominant reason. The further increase in current after subsequent cathodization was due to the *in situ* conversion of eGO to erGO on the electrode to promote conductivity. As a comparison, we calculated the EASA values of cGO-CPE, and crGO-CPE to be 0.0137 ± 0.0020 cm^2 and 0.169 ± 0.0010 cm^2.

Then, we used the commonly used probes to illustrate the electrochemical performance of the electro-activated CPE and compare its performance with that of cGO-CPE and crGO-CPE. CV responses to the $[Fe^{II/III}(CN)_6]$ probe (Fig. 5c) revealed that the pristine CPE showed both oxidative and reductive responses prior to any treatment. However, the electrode was irreversible as the peak potential difference (ΔE) value was too large (> 500 mV). When the electrode was anodized, a pair of distinct redox peaks appeared, indicating the increases in both reversibility ($\Delta E \approx 120$ mV) and sensitivity. After subsequent cathodization, the erGO-CPE exhibited further-increased peak intensity and acquired a pair of well-defined redox peaks ($\Delta E \approx 80$ mV). To verify the existence of CFs and their roles in the electrochemical performance of the CEs, we performed CV experiments with CREs. A similarity between CFs and graphenes in electrochemical activity was observed (Supplementary Fig. 8). Moreover, CFs were produced during anodization, which greatly increased the sensitivity of the electro-activated CE (Supplementary Fig. 9 and Supplementary Note 5). These results were all in good accordance with the aforementioned analyses. Furthermore, the dramatic changes in the peak shapes of the CV curves of the tested electrodes imply that the hindrance to electron transfer changes greatly after the electrochemical treatment. This may be primarily due to the microstructure brought about by the *in situ* formed eGO or erGO layer, which would create an ideal microenvironment that promotes the diffusion of the analyte (Wang et al., 2017). To further investigate the electrochemical performance of the electro-activated CE, we analysed the normalized data obtained with the above mentioned species, in Supplementary Fig. 11 and Supplementary Note 7.

Finally, we illustrated the applicability of electrochemical activation in fabricating high-performance electrochemical (bio-)sensors. As shown in Fig. 5c–d, the response currents of both eGO-CPE and erGO-CPE to H_2O_2 and $[Fe^{II/III}(CN)_6]$ were significantly increased compared to that of the pristine CPE. The response current intensities of eGO-CPE and erGO-CPE to $[Fe^{II/III}(CN)_6]$ increased by factors of ~66–247, respectively, and the responses to H_2O_2 increased by a factor of ~871 and even as much as three orders of magnitude, respectively, for eGO-CPE and erGO-CPE (Fig. 5e). It is noteworthy that the signal enhancement abilities of $[Fe^{II/III}(CN)_6]$ and H_2O_2 were obviously distinct, largely resulting from the inherent distinction between the two electrochemical analytes, namely, $[Fe^{II/III}(CN)_6]$ are negatively charged ions in a neutral buffer environment, while unconcentrated H_2O_2 is mainly present in a near neutral form. Graphene oxides are negatively charged materials in H_2O, which would reduce the accessibility of the $[Fe^{II/III}(CN)_6]$ ions. However, when the erGO layer was formed *in situ* after cathodization, the accessibility was significantly improved. In contrast, H_2O_2, a neutral species, was less pronounced in both activated CPE forms. Moreover, Supplementary Note 6, Supplementary Fig. 10, and Fig. 5 clearly show the differences and similarities in the responses to $[Fe^{II/III}(CN)_6]$ and H_2O_2 between the chemically prepared graphene-derivative-modified CPEs and their electrochemically activated counterparts. Enzyme electrodes prepared with eGO-CPE and erGO-CPE also showed comparable or even superior performance to those of cGO-CPE and crGO-CPE, taking the glucose oxidase (GOx) electrode as an example (Fig. 5f and Supplementary Fig. 10d). These phenomena can illustrate the significant difference in chemical properties between the two forms of electro-activated CPEs, suggesting the great potential for controllable *in situ* production of GO or rGO on CEs to achieve precise manipulation of the electrode surface chemistry.

4. Conclusions

In this study, we proposed that significant improvement in the performance of the electrochemically activated CEs resulted from the *in situ* formation of GO or rGO on the electrode surface. Morphological, spectral, atomic-resolution microscopy and electrochemical characterization of the microstructures produced on CEs during electrochemical activation confirmed their chemical nature as GO or rGO. Herein, we summarize the findings as the following points. i) GO was produced *in situ* during the anodization of CE, and GO can be further reduced to rGO after cathodization. ii) The anodization process would result in etching of the CE surface, which was very helpful in enhancing the electrode performance. In some cases, this effect could be utilized to remedy the low conductance of the *in situ* generated GO layer. iii) Nanosized CFs were produced on the electrode surface during anodization. Together, they exerted a significant impact on the electrochemical performance of CEs. iv) The *in situ* modified graphene derivative layer, comparing to its *ex situ* and chemically modified version, present better electrochemical sensing performances, largely resulted from the beneficial effects brought by the electrochemical etching effect involved in the former.

By utilizing the basic principles we have proposed, a general technology for graphene-functionalized carbon electrodes can be developed. Mainly due to its high controllability for surface chemistry, this technology has obvious advantages compared to existing methods, such as easy fabrication, good homogeneity of modified surfaces, good reproducibility, sensitivity and stability, weak constraints of electrode form and size, and cost effectiveness. To achieve this goal, efforts are still required to illuminate the quantitative relationship between the basic parameters of GO, rGO, and CFs generated *in situ*.

Author contributions

Y.W.L., D.M., and X.-E.Z. conceived and designed the experiments. X.-E.Z. guided the whole project. Y.W.L. and J.S. performed the experiments. Y.W.L., J.Z., J.S., and X.S.L. analysed the data. J.Z., D.M., Z.P.Z., and D.B.W. contributed reagents, materials and analysis tools. Y.W.L. and X.-E.Z. wrote the manuscript. All the authors discussed the results and commented on the manuscript.

Declaration of competing interest

The authors declare no competing interests.

Conflict of interests

The authors declare no conflict of interest.

CRediT authorship contribution statement

Yiwei Li: Conceptualization, Methodology, Validation, Formal analysis, Investigation, Data curation, Writing - original draft, Writing - review & editing, Visualization. **Juan Zhou:** Methodology, Formal analysis, Investigation, Writing - review & editing, Visualization, Data curation. **Jin Song:** Validation, Formal analysis, Investigation, Data curation. **Xiaosheng Liang:** Formal analysis, Investigation. **Zhiping Zhang:** Software, Resources. **Dong Men:** Conceptualization, Methodology, Software, Software, Data curation, Writing - review & editing, Visualization, Funding acquisition. **Dianbing Wang:** Software, Resources. **Xian-En Zhang:** Conceptualization, Methodology, Software, Resources, Writing - original draft, Writing - review & editing, Visualization, Supervision, Project administration, Funding acquisition.

Acknowledgment

This work was supported by the Key Research Program of the Chinese Academy of Science (Grant KFZD-SW-214), the Strategic Priority Research Program of the Chinese Academy of Sciences (Grant No. XDB29050100), the Youth Innovation Promotion Association of CAS (Grant 2014308) and the Open Research Fund Program of the State Key Laboratory of Virology of China (Grant 2019IOV006). We thank Di Li (East China Normal University), Xiayi Feng, and Kun Zhou for helpful discussions. Technical service from Core Facility and Technical Support, Wuhan Institute of Virology and Huazhong University of Science & Technology Analytical & Testing Centre are also acknowledged.

Appendix A. Supplementary data

Supplementary data to this article can be found online at https://doi.org/10.1016/j.bios.2019.111534.

References

Ambrosi, A., Chua, C.K., Bonanni, A., Pumera, M., 2014. Chem. Rev. 114 (14), 7150–7188.
Bagheri, H., Afkhami, A., Khoshsafar, H., Rezaei, M., Sabounchei, S.J., Sarlakifar, M., 2015. Anal. Chim. Acta 870 (1), 56–66.
Bai, L., Chen, Y., Bai, Y., Chen, Y., Zhou, J., 2017. Biomaterials 133, 11–19.
Blaedel, W.J., Jenkins, R.A., 1974. Anal. Chem. 46 (13), 1952–1955.
Bojdi, M.K., Mashhadizadeh, M.H., Behbahani, M., Farahani, A., Davarani, S.S.H., Bagheri, A., 2014. Electrochim. Acta 136, 59–65.
Bojdi, M.K., Behbahani, M., Najafi, M., Bagheri, A., Omidi, F., Salimi, S., 2015. Electroanalysis 27, 2458–2467.
Buzaglo, M., Bar, I.P., Varenik, M., Shunak, L., Pevzner, S., Regev, O., 2016. Adv. Mater. 29 (8), 1603528.
Cabaniss, G.E., Diamantis, A.A., Murphy, W.R.J., 1985. J. Am. Chem. Soc. 107 (7), 1845–1853.
Chen, K., Gao, W., Emaminejad, S., Kiriya, D., Ota, H., Nyein, H.Y.Y., Javey, K.T.A., 2016. Adv. Mater. 28 (22), 4397–4414.
Cheng, Q., Tang, J., Ma, J., Zhang, H., Shinya, N., Qin, L.C., 2011. J. Phys. Chem. C. Nanomater. Interfaces. 115 (47), 23584–23590.
Dan, T.F., Hu, I.F., Kuwana, T., 1985. Anal. Chem. 57 (14), 2759–2763.
Engstrom, R.C., 1982. Anal. Chem. 54 (13), 2310–2314.
Engstrom, R.C., Strasser, V.A., 1984. Anal. Chem. 56 (2), 136–141.
Evans, J.F., Kuwana, T.M., Henne, T., Royer, G.P., 1977. J. Electroanal. Chem. 80 (2), 409–416.
Falat, L., Cheng, H.Y., 1982. Anal. Chem. 54 (12), 2108–2111.
Gunasingham, H., Fleet, B., 1982. Analyst 107 (1277), 896–902.
Gusmão, R., Cunha, E., Paiva, C., Geraldo, D., Proença, F., Bento, F., 2016. Chem. Electro. Chem. 3 (12), 2138–2145.
Hadi, M., Rouhollahi, A., Yousefi, M., Taidy, F., Malekfar, R., 2006. Electroanalysis 18 (8), 787–792.
Heiduschka, P., Munz, A.W., Göpel, W., 1994. Electrochim. Acta 39 (14), 2207–2223.
Hosseini, H., Behbahani, M., Mahyari, M., Kazerooni, H., Bagheri, A., Shaabani, A., 2014. Biosens. Bioelectron. 59, 412–417.
Kepley, L.J., Bard, A.J., 1988. Anal. Chem. 60 (14), 1459–1467.
Lee, H., Choi, T.K., Lee, Y.B., Cho, H.R., Ghaffari, R., Wang, L., Choi, H.J., Chung, T.D., Lu, N.S., Hyeon, T., Choi, S.H., Kim, D.H., 2016. Nat. Nanotechnol. 11, 566–572.
Li, D., Müller, M.B., Gilje, S., Kaner, R.B., Wallace, G.G., 2008. Nat. Nanotechnol. 3, 101–105.
Liu, N., Luo, F., Wu, H.X., Liu, Y.H., Zhang, C., 2010. J. Chen. Adv. Funct. Mater. 18 (10), 1518–1525.
Liu, S., Zeng, T.H., Hofmann, M., Burcombe, E., Wei, J., Jiang, R.G., Kong, J., Chen, Y., 2011. ACS Nano 5 (9), 6971–6980.
Lotya, M.Y., Hernandez, P.J., King, R.J., Smith, V., Nicolosi, L.S., Karlsson, F.M., De Blighe, S., Wang, Z.M., McGovern, I.T., Duesberg, G.S., Coleman, J.N., 2009. J. Am. Chem. Soc. 131 (10), 3611–3620.
Matsumoto, M., Saito, Y., Park, C., Fukushima, T., Aida, T., 2015. Nat. Chem. 7, 730–736.
McCreery, R.L., 2008. Chem. Rev. 39 (7), 2646–2687.
Miller, C.W., Karweik, D.H., Kuwana, T., 1981. Anal. Chem. 53 (14), 2319–2323.
Parvez, K., Rincón, R.A., Weber, N.E., Chaa, K.C., Venkataraman, S.S., 2016. Chem. Commun. 52 (33), 5714–5717.
Pei, S., Wei, Q., Huang, K., M, H., Cheng, Ren, W.C., 2018. Nat. Commun. 145, 1–9.
Poon, M., McCreery, R.L., 1986. Anal. Chem. 58 (13), 2745–2750.
Rahmani, T., Bagheri, H., Behbahani, M., Hajian, A., Afkhami, A., 2018. Food Anal. Methods 11 (11), 3005–3014.
Rourke, J.P., Pandey, P.A., Moore, J.J., Bates, M., Kinloch, I.A., Young, R.J., Wilson, N.R., 2011. Angew Chem. Int. Ed. Engl. 50 (14), 3231–3235.
Santhiago, M., Maroneze, C.M., Silva, C.C.C., Camargo, M.N.L., Kubota, L.T., 2015. Chem. Electro. Chem. 2 (5), 761–767.
Santhiago, M., Strauss, M., Pereira, M.P., Chagas, A.S., Bufon, C.C.B., 2017. ACS Appl. Mater. Interfaces 9 (13), 11959–11966.
Shao, Y.L., El-Kady, M.F., Wang, L.J., Zhang, Q.H., Li, Y.G., Wang, H.Z., Mousaviae, M.F., Kaner, R.B., 2015. Chem. Soc. Rev. 44 (11), 3639–3665.
Shuhao, K., Selvakumar, P., Chen, S.M., Colloid, J., 2013. Interface Sci. 411 (1), 182–186.
Stutts, K.J., Kovach, P.M., Kuhr, W.G., Wightman, R.M., 1983. Anal. Chem. 55 (9), 1632–1634.
Taylor, R.J., Humffray, A.A., 1973. J. Electroanal. Chem. 42 (3), 347–354.
Thiruppathi, M., Thiyagarajan, N., Gopinathan, M., Zen, J.M., 2016. Electrochem. Commun. 69, 15–18.
Wang, J., Peng, T., 1986. Anal. Chem. 58 (8), 1787–1790.
Wang, J., Cai, X., Jonsson, C., Balakrishnan, M., 1996. Electroanalysis 8 (1), 20–24.
Wang, M.H., Ji, B.W., Gu, X.W., Tian, H. Ch, Kang, X.Y., Yang, B., Wang, X.L., Chen, X., Li, C.Y., 2017. J. Q. Liu. Biosens. Bioelectron. 99, 99–107.
Xiang, L., Zhang, P. Yu M.N., Hao, J., Wang, Y.X., Zhu, L., Dai, L.M., Mao, L.Q., 2014. Anal. Chem. 86 (10), 5017–5023.
Yang, X., Li, X., Ma, X., Jia, L., Zhu, L.L.D., 2013. RSC Adv. 3 (19), 6752–6755.
Yang, S., Brüller, S., Wu, Z.S., Liu, Z.Y., Parvez, K., Dong, R.H., Richard, F., Samor, P., Feng, X.L., Müllen, K., 2015. J. Am. Chem. Soc. 137 (43), 13927–13932.
Yu, P., Tian, Z.M., Lowe, S.E., Song, J.C., Ma, Z.R., Wang, X., Han, Z.J., Bao, Q.L., Simon, G.P., Li, D., Zhong, Y.L., 2016. Chem. Mater. 28 (22), 8429–8438.
Zak, J., Kuwana, T., 1982. J. Am. Chem. Soc. 104 (20), 5514–5515.
Zeinali, H., Bagheri, H., Monsef-Khoshhesab, Z., Khoshsafar, H., 2017. A. Hajian. Mat. Sci. Eng. C-Mater. 71 (1), 386–394.